Chemical Science

ROYAL SOCIETY OF CHEMISTRY

EDGE ARTICLE

View Article Online
View Journal | View Issue

Cite this: *Chem. Sci.*, 2023, **14**, 8187

All publication charges for this article have been paid for by the Royal Society of Chemistry

HAA by the first {Mn(III)OH} complex with all O-donor ligands†

Shawn M. Moore,[a] Chen Sun,[a] Jennifer L. Steele,[a] Ellen M. Laaker,[a] Arnold L. Rheingold[b] and Linda H. Doerrer *[a]

There is considerable interest in $MnOH_x$ moieties, particularly in the stepwise changes in those O–H bonds in tandem with Mn oxidation state changes. The reactivity of aquo-derived ligands, $\{MOH_x\}$, is also heavily influenced by the electronic character of the other ligands. Despite the prevalence of oxygen coordination in biological systems, preparation of mononuclear Mn complexes of this type with all O-donors is rare. Herein, we report several Mn complexes with perfluoropinacolate $(pin^F)^{2-}$ including the first example of a crystallographically characterized mononuclear {Mn(III)OH} with all O-donors, $K_2[Mn(OH)(pin^F)_2]$, **3**. Complex **3** is prepared *via* deprotonation of $K[Mn(OH_2)(pin^F)_2]$, **1**, the pK_a of which is estimated to be 18.3 ± 0.3. Cyclic voltammetry reveals quasi-reversible redox behavior for both **1** and **3** with an unusually large ΔE_p, assigned to the Mn(III/II) couple. Using the Bordwell method, the bond dissociation free energy (BDFE) of the O–H bond in $\{Mn(II)–OH_2\}$ is estimated to be 67–70 kcal mol^{-1}. Complex **3** abstracts H-atoms from 1,2-diphenylhydrazine, 2,4,6-TTBP, and TEMPOH, the latter of which supports a PCET mechanism. Under basic conditions in air, the synthesis of **1** results in $K_2[Mn(OAc)(pin^F)_2]$, **2**, proposed to result from the oxidation of Et_2O to EtOAc by a reactive Mn species, followed by ester hydrolysis. Complex **3** alone does not react with Et_2O, but addition of O_2 at low temperature effects the formation of a new chromophore proposed to be a Mn(IV) species. The related complexes $K(18C6)[Mn(III)(pin^F)_2]$, **4**, and $(Me_4N)_2[Mn(II)(pin^F)_2]$, **5**, have also been prepared and their properties discussed in relation to complexes **1**–**3**.

Received 14th April 2023
Accepted 5th July 2023

DOI: 10.1039/d3sc01971c

rsc.li/chemical-science

Introduction

Manganese-dependent enzymes effect both oxidation and reduction reactions involving O_2. From the dioxygenation of *cis*, *cis*-1,4-pentadiene-containing fatty acids to alkyl hydroperoxides by manganese lipoxygenases (MnLOX),[1–3] to the reduction of water in the oxygen evolving cluster (OEC) of photosystem II (PSII),[4,5] manganese is essential for both breaking and forming the O=O bond. Mn-oxo, -hydroxo, and -aquo species, collectively $\{MnOH_x\}$ (x = 0, 1, 2), have been proposed to play critical roles in the function of several of these enzymes (Chart 1). For example, a mononuclear Mn(III)–OH moiety has been implicated in the catalytic cycle of Mn-superoxide dismutase (MnSOD),[6] which defends aerobic organisms from reactive oxygen species by catalyzing the disproportionation of superoxide into H_2O_2 and O_2. Likewise, $\{MnOH_x\}$ species have also been proposed in the active sites of both Mn-lipoxygenase and the OEC.[7,8]

Importantly, each of these enzymes uses proton-coupled electron-transfer (PCET) reactions. The Mn center shuttles among the +2, +3, and +4 oxidation states while oxo, hydroxo, or aquo moieties are (de)protonated. This separable e^-/H^+ transfer reactivity is distinct from concerted e^-/H^+ transfer, also called a hydrogen atom transfer (HAT). In some cases, PCET mechanisms at $\{MOH_x\}$ sites cleave thermodynamically strong (>100 kcal mol^{-1}) and kinetically inert C–H bonds.[9] For example, Fe and Cu dependent methane monooxygenases catalyze the oxidation of CH_4 (C–H BDFE = 105 kcal mol^{-1})[10] to CH_3OH *via* a PCET mechanism that invokes metal-oxo, -hydroxo, and -aquo species.[11]

As our understanding of the role of $\{MnOH_x\}$ species in biology has grown, so too has interest in the synthesis of metal complexes that mimic the structure and particularly the function of these enzymes. Histidine N-ligation is extremely widespread in Nature, including the MnLOX and MnSOD enzymes as shown in Chart 1. Therefore, several $\{MnOH_x\}$ complexes with N-donor ligands as models for histidine that can oxidize C–H and/or O–H bonds have been prepared, a selection of which are shown in Chart 2. The Borovik,[12,13] Goldberg,[14] Jackson,[15] Kovacs,[16] Nam,[17] and Stack[18] groups have each prepared

[a]*Boston University, Chemistry Department, 590 Commonwealth Avenue, Boston, Massachusetts 02215, USA. E-mail: doerrer@bu.edu*

[b]*University of California, San Diego Department of Chemistry and Biochemistry, 9500 Gilman Drive, La Jolla, California 92093, USA*

† Electronic supplementary information (ESI) available. CCDC 2246386–2246390. For ESI and crystallographic data in CIF or other electronic format see DOI: https://doi.org/10.1039/d3sc01971c

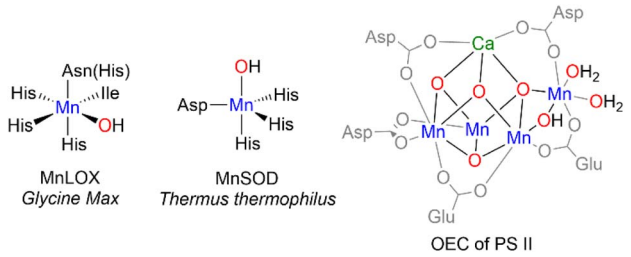

Chart 1 Primary coordination spheres of three Mn containing enzymes.

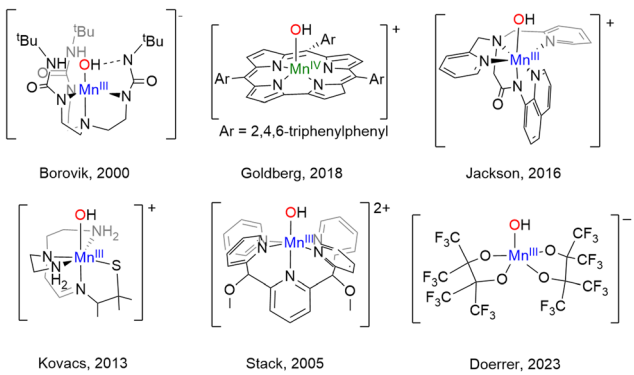

Chart 2 Selected {Mn(OH)} complexes.

mononuclear {$MnOH_x$} complexes supported by amino, amido, and/or pyridyl ligands from Mn(II) starting materials using oxidants such as O_2, H_2O_2, or PhIO. The reactivity of these complexes is dependent on the N-donor ligands. Donation from nitrogen lone pairs into the Mn=O π^* orbital can weaken the Mn=O bond rendering it more reactive. High reactivity in model complexes, however, often leads to intra- or intermolecular ligand oxidation and makes isolation and characterization of reactive species a challenge.

In contrast to the N-donor rich coordination of MnLOX and MnSOD, the OEC shown on the right of Chart 1 features a $CaMn_4O_5$ cluster with Mn in an all O-coordination environment made up of -oxo, -hydroxo, and -aquo ligands in addition to aspartate and glutamate residues.[4] Model complexes (structural, spectroscopic, or functional) with exclusively O-donor environments are much less common than their N-donor counterparts. To the best of our knowledge, the four-coordinate complex, $[Mn(IV)(O)(ditox)_3]^-$, from the Nocera[19] group remains the only structurally characterized example of an O-coordinated mononuclear Mn complex with C–H bond activation abilities. In the trianionic, $\sim C_{3v}$ ligand field of the tris-ditox environment, the Mn(IV)=O unit is sufficiently stable to permit isolation, but only reacts with C–H bonds having BDE <85 kcal mol^{-1}. Computational studies have attributed the enhanced reactivity of this complex to low energy exited states that lower the barrier for reaction compared to the ground state.[20] The dearth of oxidatively active O-ligated Mn complexes is due in large part to synthetic challenges posed by O-donor ligands. Neutral O-donors like H_2O, ketones, and ethers form relatively weak Mn–O bonds leading to lability. Anionic alkoxides form stronger bonds, but π-donation from the oxygen lone pairs can lead to less reactive, coordinatively saturated alkoxide-bridged complexes. Using bulky alkoxides can prevent bridging, but excess bulk can inhibit substrate binding and prevent reactivity.[21]

Recently, the Kulik group carried out a computational screen of over 2500 mid-row 3*d* transition-metal (Cr, Mn, Fe, Co) complexes to uncover trends in reactivity.[22] They found that stabilizing high-spin ground states enhances catalytic activity by enabling spin-allowed transitions to or from closed-shell substrates. Their analysis identified weak-field, O-coordinating ligands as promising candidates for future design of Fe(II) C–H activation catalysts, and for transition metal catalysts in general. This study underscores the need to develop ligand systems which leverage the promising effects of O-donor ligation on catalyst reactivity without the challenges posed by alkoxide ligation.

In the last decade, our group has demonstrated the ability of fluorinated alkoxides to support 3*d* metals in a variety of oxidation states and geometries.[23–29] These ligands can stabilize the high oxidation states necessary for oxidation chemistry and the high-spin states that the Kulik group[22] and others[20,30] have shown to be beneficial to catalysis. We have prepared a highly-unusual square-planar $S = 1$ Co(III) complex,[24] a high-spin $S = 2$ Fe(II) complex,[27] and a bis-(μ_2-OH) bridged V(IV) dimer that results from HAA (hydrogen atom abstraction) from alcohols.[31] This latter process is part of catalytic oxidative alcohol dehydrogenation.[31] Ligand fluorination decreases alkoxide bridging of metal centers by reducing π-bonding and Lewis basicity *via* the inductive effect. Fluorinated alkoxides are oxidatively robust when compared to their hydrogenated analogues due to the greater stability of C–F bonds *versus* C–H bonds. Ligand fluorination also increases water tolerance *via* the lower alcohol pK_a values of up to 14 orders of magnitude.[32] In some cases, transition metal complexes with fluorinated ligands have been able to oxidize C–H[31,33] and O–H bonds.[31]

In this work we present the synthesis and characterization of several Mn complexes supported by the perfluoropinacolate (pin^F) ligand. These complexes have all O-donor coordination leading to anionic complexes with supporting cations that form non-covalent $K^+\cdots O$ and $K^+\cdots F$ interactions with ligand and solvent molecules. These non-covalent interactions allowed, for the first time, isolation and crystallographic characterization of a {Mn(III)OH} complex with all O-donors, **3**. This compound is a precursor to a potent oxidant of Et_2O.

Results and discussion

Syntheses and crystallographic structures

The increased acidity afforded by perfluorination allows some pin^F complexes to be prepared in water on the benchtop. Combining an aqueous solution of $MnSO_4$ with an aqueous solution containing two equivalents of H_2pin^F and four of KOH in air affords a pink solution that darkens to a deep maroon over several hours, indicative of oxidation from Mn(II) to Mn(III) (Scheme 1, top). Purification results in brick red needles of K

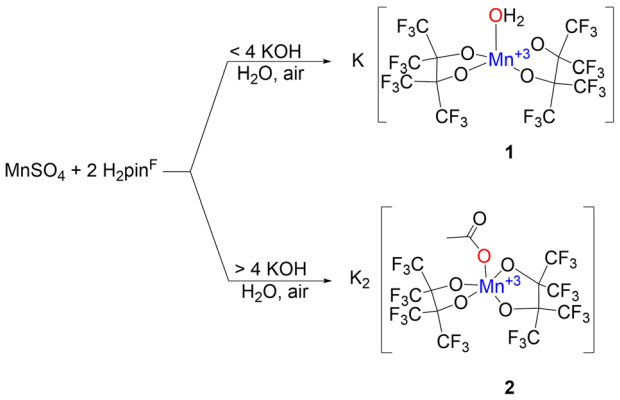

Scheme 1 Synthesis of **1** (top) and **2** (bottom).

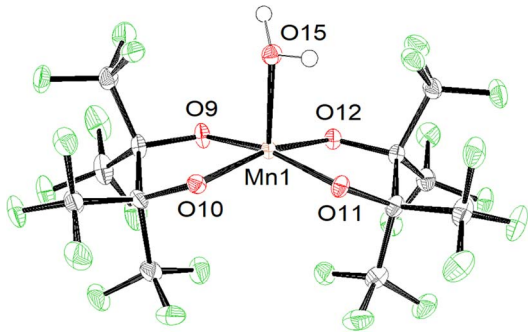

Fig. 1 ORTEP of the **1** anion with cations and solvent molecules omitted for clarity. Ellipsoids are shown at the 50% probability level.

$[Mn(OH_2)(pin^F)_2]$, **1**, that has a square pyramidal Mn(III) center with $\tau_5 = 0.01$ in an asymmetric unit containing three molecules of **1** and seven H_2O (Fig. S1†). One of the Mn-based anions is shown in Fig. 1.

One consequence of the use of alkoxides as ligands is the resulting complexes are all anions allowing for cations to play a role in structure and reactivity. Our group has previously described how K···O and K···F interactions influence the solubility, nuclearity, and geometry of these complexes.[23] The chemistry community is increasingly interested in how non-covalent interactions with Lewis acidic, redox-inactive cations tune the reactivity of metal-oxo, -hydroxo, and -aquo complexes.[34,35] Fluorinated alkoxide complexes provide an excellent model system to utilize these effects. For example, in **1** the three Mn–OH_2 bonds average 2.18 Å, and the Mn–O_{pin^F} bonds are between 1.883(3) Å and 1.890(3) Å (Table S1†). The Mn(3)–O(5) bond is roughly 0.05 Å longer, however, than the other two Mn–OH_2 bonds due to a 2.744(3) Å interaction between O(5) and K(3). Samples of **1** can be dried under vacuum and gentle heat to remove the lattice H_2O molecules, but elemental analysis confirms that one molecule of H_2O per Mn remains intact.

Using more than four equivalents of KOH per Mn when deprotonating H_2pin^F initially results in the formation of an orange precipitate, but after stirring overnight the solution darkens to a deep maroon (Scheme 1, bottom). Purification

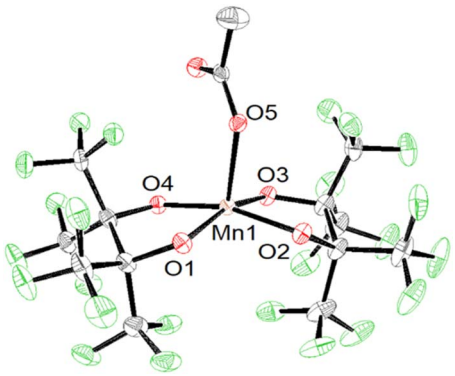

Fig. 2 ORTEP of the anion of **2** with cations and solvent molecules omitted for clarity. Ellipsoids are shown at the 50% probability level.

gives purple X-ray quality needles overnight which SCXRD reveal to be an unexpected acetate complex, $K_2[Mn(OAc)(pin^F)_2]$, **2** shown in Fig. 2. The asymmetric unit contains two molecules of **2** and two Et_2O (Fig. S2†). The Mn(III) ion is square pyramidal with a τ_5 value of 0.01. The Mn–OAc bonds average 2.09 Å, 0.1 Å shorter than the Mn–OH_2 bonds in **1**. The Mn–O_{pin^F} bonds are between 1.879(3) Å and 1.926(3) Å (Table S1†). Once again we see the structural role played by non-covalent interactions with cations as the two anions are bridged by K···O_{pin^F} and K···OAc interactions with K(3) and K(4) that make both K^+ ions seven coordinate (Fig. S2†).

The presence of OAc^- as a ligand was unexpected as there is no obvious source of a C_2 fragment and this result is reproducible with yields as high as 58% ruling out contamination as the source. We hypothesize that OAc^- is the result of oxidation of the crystallization solvent Et_2O to EtOAc followed by hydrolysis to yield EtOH and OAc^- (Scheme 2). There are numerous examples of Mn(III) complexes mediating oxidation reactions, most notably in the case of $\{Mn(OAc)_3\}$ which has been heavily studied for the promotion of oxidative free-radical reactions between carbonyl compounds and unsaturated molecules to form cyclic products.[36] Busch and co-workers isolated the Mn(IV) complex $[Mn(Me_2EBC)(OH)(OAc)]^+$ with an unexpected acetate ligand proposed to be derived from oxidation of the reaction solvent, EtOH, by $[Mn((Me_2EBC))(OH)_2]^+$.[37]

Formation of **2** in the presence of excess base led us to investigate deprotonation of **1** under more controlled conditions. Under a N_2 atmosphere reacting **1** with an equivalent of $KN(SiMe_3)_2$ in methyl *tert*-butyl ether (MTBE) (Scheme 3) immediately causes a color change from red to blue. Purification resulted in the formation of blue single crystalline blocks shown by SCXRD to be a rare example of a mononuclear Mn(III)

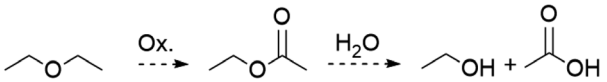

Scheme 2 General reaction by which Et_2O may be oxidized to ethyl acetate then hydrolysed to ethanol and acetic acid that is proposed to be the source of the OAc^- anion in **2**.

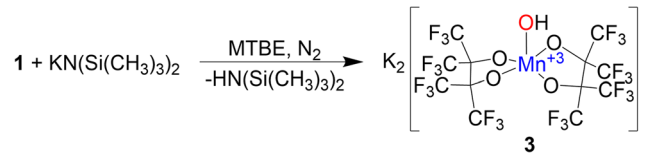

Scheme 3 Synthesis of **3**.

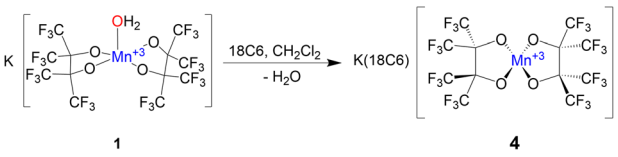

Scheme 4 Synthesis of complex **4**.

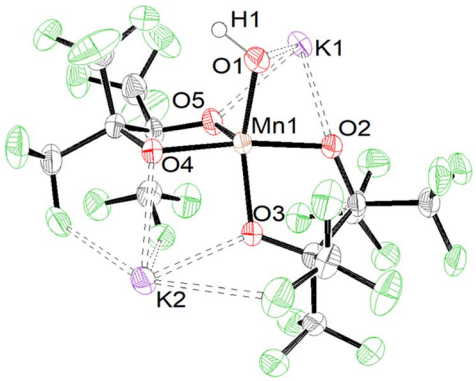

Fig. 3 ORTEP of **3** with solvent molecules omitted for clarity. Ellipsoids are shown at the 50% probability level.

hydroxide complex $K_2[Mn(OH)(pin^F)_2]\cdot 3$ MTBE, **3**·3 MTBE (Fig. 3).

Like **1** and **2** the Mn atom in **3** is square pyramidal, although more distorted, with a τ_5 value of 0.35. The Mn–OH bond in **3** is 1.857(3) Å (Table S1†), ~0.3 Å shorter than the Mn–OH_2 bond in **1** and is consistent with that found in other Mn(III) hydroxide complexes.[12,15–18,38] Complex **3** is air and moisture sensitive but remains stable in the solid state over months in a N_2 filled dry box. Polar coordinating solvents such as Et_2O, THF, or MTBE are required to solubilize **3** which does not dissolve in CH_2Cl_2 or toluene. In MeCN, **3** irreversibly changes color from blue to red/brown which we hypothesize is the result of nucleophilic attack on the nitrile group. For this reason, all remaining characterization and reactivity with **3** was performed in THF. Complex **3** is the first example of a {Mn(III)(OH)} complex with all O-donors. No other {Mn(III)OH} is reported to act as a nucleophile, a property that may be attributable to the anionic charge of the complex enabled by the use of alkoxide ligands. The synthesis of **3** is unique among {Mn(III)OH} complexes in that it is achieved by deprotonation of the corresponding {Mn(III)OH_2} complex. Existing complexes of this type are prepared by the oxidation of a Mn(II) complex with O_2 or PhIO.

Complex **3** crystalizes in pairs (Fig. S3†) of crystallographically identical molecules bridged by K···O_{pin^F}, K···OH, and K···F interactions. While we have described the hydroxide as terminal, it is formally a μ_3-OH in the solid state with two K···OH interactions measuring 2.655(3) Å and 3.110(4) Å, but these bonds are unlikely to persist when **3** is dissolved in polar organic solvents. The distances in **3** are consistent with the few crystallographically characterized K(μ_2-OH)TM structures, *e.g.*, K(DME)[tpa^{Mes}Fe(OH)].[40] Attempts to encapsulate the K^+ ions with DME or 18C6 invariably lead to degradation of **3** demonstrating the importance of the K···O and K···F interactions in allowing the isolation of **3**. The hydroxyl proton was located in the difference map and was refined independently to a length of 1.02(15) Å.

The solid-state structures of **1–3** demonstrate how non-covalent interactions with "naked" K^+ can play integral roles in bonding and even allow for the isolation of reactive species by stabilizing metal hydroxide complexes. Interested in how reducing these interactions would alter the structure of the resulting complex, we chose to encapsulate the K^+ in **1** with a crown ether. Complex **1** is insoluble in CH_2Cl_2, but addition of one equivalent of 18C6 to a suspension of **1** in CH_2Cl_2 allows for complete solubility. After filtering and drying the red solution an orange powder is produced which was subsequently crystalized from dry CH_2Cl_2 resulting in orange crystals of K(18C6)[Mn(pin^F)$_2$], **4**, in greater than 80% yield (Scheme 4).

SCXRD of **4** shows a square-planar Mn(III) center (Fig. 4) with two pairs of equivalent Mn–O_{pin^F} bonds measuring 1.8588(15) Å and 1.8574(14) Å respectively (Table S2†). None of the K···O and K···F interactions seen in the structures of **1–3** persist in **4** (Fig. S4†). To the best of our knowledge, **4** is the only crystallographically characterized {Mn(III)O_4} complex with square planar geometry (τ_4 = 0.00) and this geometry is perhaps influenced by a Jahn–Teller distortion in this high-spin ($S = 2$) d^4 ion. Complex **1**, with its naked K^+, is resistant to dehydration even under vacuum and mild heat, while transient {K(18C6)}[Mn(OH_2)(pin^F)$_2$] is easily dehydrated under a gentle air stream at RT. We attribute this contrast in ligand lability to K···O_{pin^F} interactions in **1** resulting in a more electrophilic metal center. Without the K···O_{pin^F} interactions in **4**, lone pairs from the alkoxide ligands donate more strongly into the Mn center and reduce its Lewis acidity.

In addition to the four Mn(III) complexes discussed above, the Mn(II) complex $(Me_4N)_2[Mn(pin^F)_2]$, **5**, was prepared

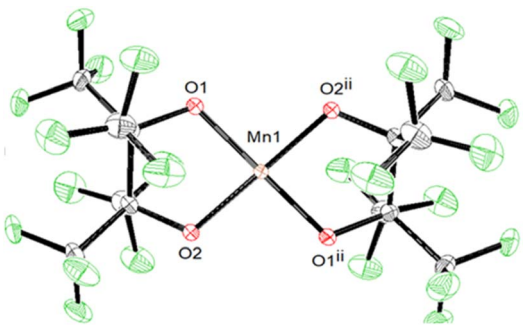

Fig. 4 ORTEP of the anion of **4**. Ellipsoids are shown at the 50% probability level.

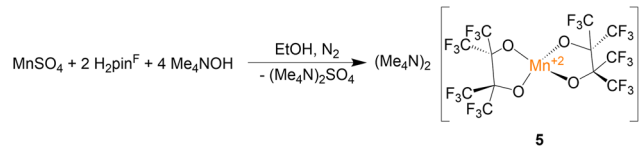

Scheme 5 Synthesis of complex **5**.

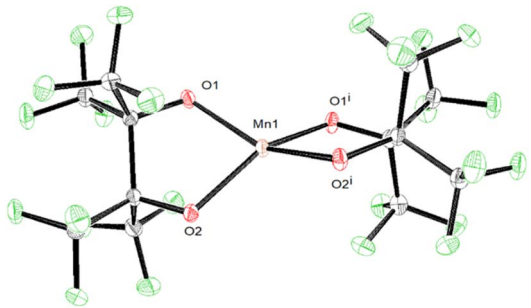

Fig. 5 ORTEP of the anion of **5** with cations and solvent molecule excluded for clarity. Ellipsoids are shown at the 50% probability level.

according to Scheme 5. This colorless compound consists of a pseudo-tetrahedral anion (τ_4 = 0.43), shown in Fig. 5, with Mn–O_{pin^F} bonds that average 2.042 Å which is 0.18 Å longer than in **4** (Table S2†). The anions of **4** and **5** differ by just a single electron but show a dramatic difference in geometry. There are no interactions between the Me_4N^+ and the anion (Fig. S5†).

Proton, electron, and H-atom transfer

Compound **1** can be deprotonated by titrating a THF solution of **1** (Fig. 6, red) with KOtBu which affords **3** (Fig. 6, blue) and displays beautiful isosbestic behavior. More than one equivalent of KO^{t}Bu is required to fully react with **1** suggesting that an equilibrium is established between the Mn–OH_2 species and KO^{t}Bu. For this to be true, the pK_a of the Mn bound H_2O must be similar in value to that of HO^{t}Bu. Efforts to directly determine the pK_a of the coordinated H_2O in **1** by spectrophotometric titration were thwarted by the reactivity of **3** with MeCN and DMSO which have well established pK_a scales. We instead bracketed the pK_a by reactions with stoichiometric amounts of bases with known pK_a values. One equivalent of $KN(SiMe_3)_2$ (pK_a = 26) is sufficient to completely deprotonate **1**, while one equivalent of KO^{t}Bu (pK_a = 17) only results in partial deprotonation (Fig. 6). Similarly, reaction with up to 30 equivalents of 7-methyl-1,5,7-triazabicyclo[4.4.0]dec-5-ene (MTBD, pK_a = 18.0) results in only partial conversion to **3** (Fig. S6†). Based on these observations, we estimate the pK_a of the O–H bond in **1** to be 18.3 ± 0.3 in THF.

Determining the pK_a of a metal bound H_2O is extremely challenging. Complex **1** is the only {Mn(III)OH_2} complex for which characterization has been performed in THF. Nam and co-workers have measured the pK_a of the H_2O in $[Mn(III)(OH_2)(dpaq^H)]^+$ to be 6.78 in MeCN.[39] The Kovacs group found that pK_a = 5.3 in H_2O for $[Mn(II)(S^{Me_2}N_4(tren))(H_2O)]^+$ which results from PCET by $[Mn(III)(S^{Me_2}N_4(tren))(OH)]^+$.[16] There have also been pK_a measurements reported for metal bound hydroxide Mn–O(H) complexes. Borovik and co-workers have reported the pK_a of $[Mn^{III}H_3buea(OH)]^-$ to be 28 in DMSO.[41] The Borovik group also reported that 22 < pK_a < 24.4 of $[Mn(III)H_3bpuea\text{-}R(OH)]^{2-}$ (R = OMe, H, F, Cl, CF_3, 5F) in DMSO with the more electron withdrawing ligands resulting in a lower pK_a.[42] The pK_a of a metal bound water or hydroxide is anti-correlated with an increase in reduction potential. Having a large pK_a can allow a complex to abstract H atoms despite unfavorable thermodynamics for electron transfer. For example, the basicity of the oxido ligand in $[Mn^{III}H_3buea(O)]^{2-}$ allows it to abstract H-atoms from 9–10 dihydroanthracene (DHA, $BDFE_{C-H}$ = 76 kcal mol^{-1}) despite its unfavorable reduction potential of −2.0 V *vs.* $Fc^{+/0}$.[41] One would expect that the pK_a of Mn–OH > Mn–OH_2 and, thus, that the Mn–O would be a better oxidant.

The redox behavior of **1** and **3** was investigated with cyclic voltammetry, as shown in Fig. 7. The voltammogram for **1** in THF (Fig. 7, red) shows a quasi-reversible feature with $E_{p,c}$ = −0.98 V and $E_{p,a}$ = 1.43 V at a scan rate of 1 V s^{-1}. Potentials have been referenced to $Fc^{+/0}$ using an internal standard and the reversibility was consistent over a range of scan rates (Fig. S7–

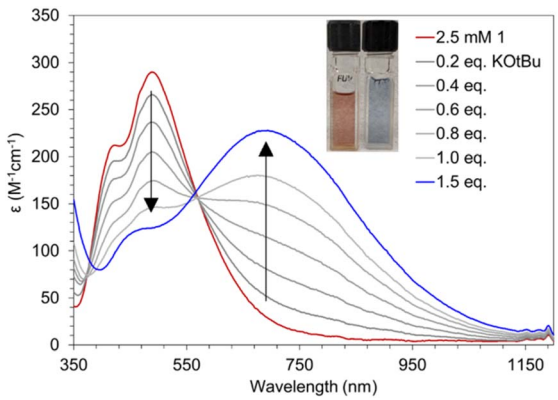

Fig. 6 UV-vis spectra of titration of **1** (2 mM) to form **3** with portions of KO^{t}Bu in THF.

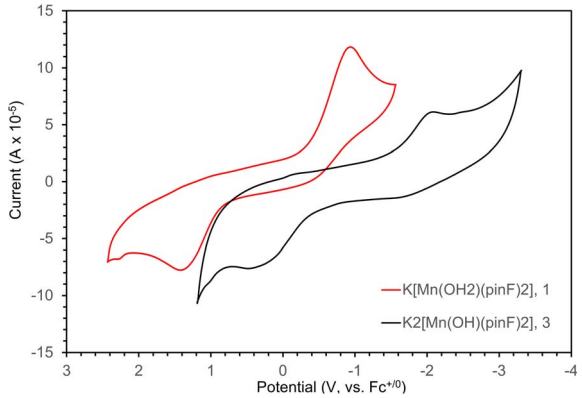

Fig. 7 Cyclic voltammograms for 5 mM solutions of **1** (red) and **3** (black) in THF with 250 mM $TBAPF_6$ as a supporting electrolyte. Scan rate is 1 V s^{-1} and potentials are referenced to $Fc^{+/0}$.

S9†). The voltammogram displays an unusually large peak separation of 2.41 V attributed to a large inner sphere reorganization (loss of coordinated H_2O) that occurs upon reduction from Mn(III) to Mn(II). This proposal is supported by the difference in geometry (square planar *vs.* tetrahedral) for the $[Mn(pin^F)_2]^{n-}$ anion in Mn(III) **4** and Mn(II) **5** respectively. In a less coordinating solvent such as the atypical 60 : 40 CH_2Cl_2 : Et_2O mixture (Fig. S10†) a single broad reduction event is observed with $E_{p,c} = -1.70$ V corresponding to the reduction of five-coordinate Mn(III). In the oxidative direction, however, two events can be seen at $E_{p,a} = -0.23$ V and -0.033 V corresponding to the oxidation of both a proposed transient solvated Mn(II) and the known four-coordinate species, indicative of weak ligand binding in the axial position upon reduction to Mn(II) (Scheme S11†).

The voltammogram of **3** (Fig. 7, black) also displays a quasi-reversible feature with a reduction event at -2.05 V coupled to a broad oxidative feature at 0.39 V. The measured potentials were referenced to $Fc^{+/0}$ using a $CoCp_2^*$ internal standard and the reversibility confirmed over scan rates of 0.1 to 2.0 V s^{-1} (Fig. S12–S14†). Once again, the peak separation of 2.44 V is unusually large and is likely due to a chemical transformation upon reduction to Mn(II). Complex **3** is more difficult to reduce than **1** consistent with the increase in energy necessary to reduce a complex with a greater negative charge.

The hydrogen atom abstraction (HAA) ability of **3** was investigated with stoichiometric amounts of substrates with weak X–H bonds (X = C, N, O). Reactions with 1,2-diphenylhydrazine (DPH, $BDFE_{N-H} = 64.0$ kcal mol^{-1}) are complete after roughly 100 minutes at RT producing azobenzene and $[Mn(II)(pin^F)_2]^{2-}$ along with an equivalent of water (Fig. 8). Similarly, reactions with 1-hydroxy-2,2,6,6-tetramethylpiperidine (TEMPOH, $BDFE_{O-H} = 66.5$ kcal mol^{-1} in MeCN) are rapid at RT to produce the (2,2,6,6-tetramethylpiperidin-1-yl)oxyl (TEMPO) radical as evidenced by the characteristic feature at 440 nm (Fig. S15†). Oxidation of TEMPOH is strongly biased to occur *via* PCET due to its thermodynamically unfavorable pK_a (41 in MeCN) and one e^- reduction potential (-1.85 V *vs.* $Fc^{+/0}$ in MeCN).[43] Reactivity of **3** with TEMPOH supports a PCET mechanism for other reactions but does not rule out asynchronous H^+/e^- transfer. Complex **3** also reacts with 2,4,6-tri-*tert*-butylphenol (2,4,6-TTBP, O–H BDFE = 74.4 kcal mol^{-1}).[43] Monitoring the reaction of **3** with 10 eq. 2,4,6-TTBP by electronic absorption spectroscopy shows the decay of **3** and the formation of the 2,4,6-tri-*t*-butylphenoxyl radical ($\lambda_{max} = 630$ nm, Fig. 9).

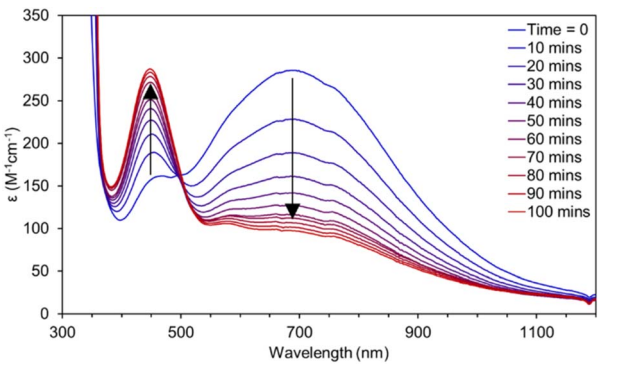

Fig. 8 UV-vis spectra for the reaction of a 2 mM solution of **3** in THF with 1/2 equivalent of 1,2-diphenylhydrazine.

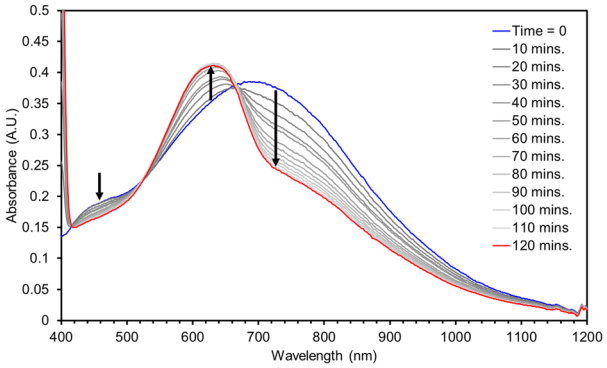

Fig. 9 UV-vis spectra for the reaction of a 2 mM solution of **3** in MTBE with 10 eq. TTBP.

No reaction has been observed at RT with either the C–H bonds of 9,10-dihydroanthracene (DHA, $BDFE_{C-H}$ = 72.9 kcal mol^{-1}) or 1,4-cyclohexadiene (CHD, $BDFE_{C-H}$ = 67.8 kcal mol^{-1}). Lack of reaction with DHA or CHD despite the ability to oxidize the stronger O–H bond in 2,4,6-TTBP suggests that substrate BDFE may not be the perfect descriptor for understanding the thermodynamics of HAA by **3**.

$$BDFE = 23.06E^\circ + 1.37(pK_a) + C_{(g,sol)} \quad (1)$$

The O–H bond BDFE in the hypothesized, transient {Mn(II)OH_2} moiety can be calculated using the Bordwell equation (eqn (1)).[43,44] The $C_{(g,sol)}$ term is a composite, solvent dependent, free-energy constant that represents the energy of solvation for an H-atom in the solvent of interest (59.9 in THF).[43] For systems which undergo ideal one e^- redox processes, E° can be approximated as $E_{1/2}$ from CV. However, the large ΔE in the CV of **1** casts doubt on the reliability of $E_{1/2}$ as an approximation of

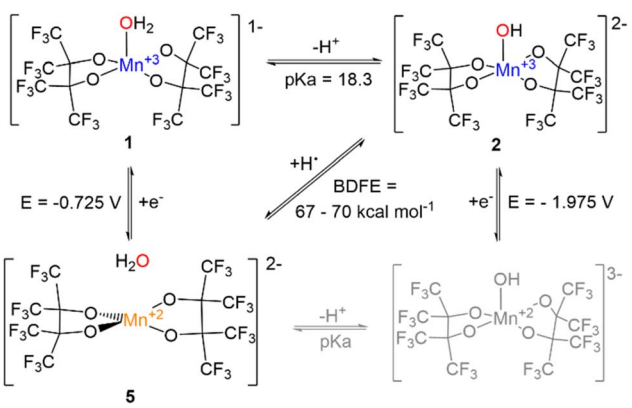

Scheme 6 Bordwell scheme depicting the proton, electron, and hydrogen atom transfer events and their respective thermodynamic parameter for the $[Mn(OH_x)(pin^F)_2]^{n-}$ system. Gray indicates a proposed, not isolated species.

Table 1 Thermochemical parameters for {Mn(III)OH} complexes that oxidize C–H, N–H, or O–H bonds

Complex	pK_a Mn(III)OH_2	E^{a} (V)	Solvent	BDFE (kcal mol^{-1})	Ref.
[Mn(III)($S^{Me_2}N_4$(tren))(OH)]$^+$	21.2[b]	−0.6	MeCN	70.1[b]	16
[Mn(III)(OH)(dpaq^{H})]$^+$	6.8	−0.73[c]	MeCN	79.4	39,45
[Mn(III)(OH)(dpaq^{2me})]$^+$	20[c]	−0.62[c]	MeCN	80.9	45
[Mn(III)(OH)(PY5)]$^{2+}$	13[f]	0.186[d]	MeCN	82	18
[Mn(OH)(pin^{F})$_2$]$^{2-}$	18.3 ± 0.3	−0.725[e]	THF	67–70	This work

[a] Potentials *vs.* $Fc^{+/0}$. [b] Estimated in MeCN. [c] Calculated. [d] Measured *vs.* SHE and converted to $Fc^{+/0}$. [e] $E_{p,c}$. [f] In MeCN.

$E°$. If instead we choose E at $I_{p,c}$ from the voltammogram recorded at 100 mV s^{-1} (−0.725 V) we calculate a BDFE of 67–70 kcal mol^{-1}. This range does not overlap exactly with the demonstrated reactivity with 2,4,6-TTBP (BDFE = 74.4 kcal mol^{-1}). The value in our Bordwell equation with the greatest uncertainty is the reduction potential of {Mn(III)$(OH)_2$}, **1**, to {Mn(II)}, **5**, which is accompanied by a change in geometry and coordination number. With this uncertainty, the calculated BDFE range is reasonable.

The Bordwell thermochemical cycle for the H-atom transfer reaction is shown in Scheme 6. Complex **3** is the only {Mn(III)(OH)} complex for which thermodynamic data have been reported in THF. While pK_a and $E_{1/2}$ values are strongly solvent dependent, it has recently been shown that BDFEs are nearly independent of solvent.[43]

For example, the measured BDFE of the O–H bond in TEMPOH averages 65.0 ± 1.3 kcal mol^{-1} in solvents whose dielectric constants differ by 38 units (MeCN *vs.* hexane). The known Mn(II)OH_2 complexes which result from HAT by a {Mn(III)OH} complex for which an O–H BDFE has been reported is limited to those shown in Table 1. The oxidizing power of **3** is comparable to [Mn(III)($S^{Me_2}N_4$(tren))(OH)]$^+$ from the Kovacs group,[16] and [Mn(III)(OH)(dpaq^{H})]$^+$ and its methylated analogue from the Jackson group.[15,45] [Mn(III)(OH)(PY5)]$^{2+}$ from the Stack group is unique among these complexes as it is the only example reported to oxidize C–H bonds.[18]

Based on the measurements described above and the observed stability of **3** in Et_2O under N_2 it is unlikely that **3** is responsible for the oxidation of Et_2O that results in **2**. Because the synthesis of **2** is performed in air, if **3** is formed in solution, it could react with O_2 to form a higher valent Mn species capable of oxidizing Et_2O. To test this hypothesis a solution of **3** prepared under N_2 in either Et_2O (solid lines) or MTBE (dotted lines) was cooled to −100 °C in the spectrophotometer and the spectra recorded (Fig. 10, blue traces). Next, excess O_2 was added and in both solvents a new chromophore appears with λ_{max} = 550 nm that reaches a maximum absorbance after 50 minutes at −100 °C (Fig. 10, red traces). The solution was then gradually warmed in 20 °C increments. At −80 °C no change was observed, but at −60 °C the chromophore has decayed to a new spectrum that does not match any of the chromophores discussed here (Fig. 10, black traces). Crucially, the chromophore shows much greater decay in MTBE than in Et_2O. Further warming to −40 °C did not change the spectrum of this decayed product. Efforts to isolate this intermediate and obtain more indirect evidence *via* reactivity are underway.

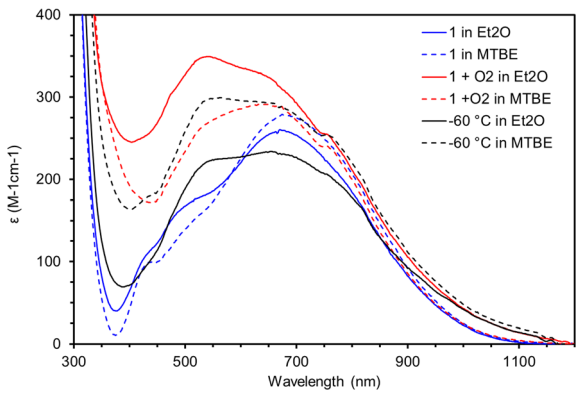

Fig. 10 UV-vis spectra for the addition of O_2 to **3** (2 mM) at −100 °C in MTBE (dotted) and Et_2O (solid). After O_2 addition the solution was allowed to rest in the spectrophotometer at −100 °C before warming.

Conclusions

Described here are the synthesis and structural characterization of five Mn complexes supported by the perfluoropinacolate ligand. The synthesis of K[Mn(OH_2)(pin^{F})$_2$], **1**, and K(18C6)[Mn(pin^{F})$_2$], **4**, demonstrates the dependence of water ligand lability on cation encapsulation and provides in **4** the first example of a {Mn(III)O_4} complex with ∼D_{4h} geometry. The Mn(II) complex $(Me_4N)_2$[Mn(pin^{F})$_2$], **5**, was synthesized and revealed by SCXRD to have a ∼T_d geometry in contrast to the one electron oxidized product **4**. When performed in the presence of excess base, the synthesis of **1** results in K_2-[Mn(OAc)(pin^{F})$_2$], **2**, with an unexpected acetate ligand proposed to be the result of oxidation of Et_2O by an air and water tolerant oxidant. The dependence of this reaction on the amount of base used led us to deprotonate **1** under controlled conditions resulting in K_2[Mn(OH)(pin^{F})$_2$], **3**, a rare example of a crystallographically characterized mononuclear {Mn(III)OH} complex, the first with an all O-donor environment and the only anion. The redox properties of **1** and **3** were investigated with cyclic voltammetry which reveals quasi-reversible redox behavior with exceptionally large ΔE that results from a change in geometry and/or composition upon reduction for both complexes. This observation is supported by the differing geometries of **4** and **5** in the solid-state. The pK_a of the OH_2 ligand in **1** is estimated to be 18.3 ± 0.3 by reaction with

stoichiometric amounts of bases. Complex **3** oxidizes the N–H and O–H bonds *via* HAA. The BDFE of the O–H bond in transient {Mn(II)–OH_2} formed when **3** abstracts an H-atom is 67–70 kcal mol^{-1}. While **3** is unable to oxidize Et_2O on its own, low temperature addition of O_2 to solutions of **3** results in the formation of a new chromophore which decays upon warming. The identity of this proposed Mn(IV) chromophore is still under investigation. This system is the first all O-donor Mn complex shown to oxidize C–H bonds.

Data availability

All relevant data are available from the corresponding authors upon reasonable request.

Author contributions

S. M. M. – investigation, writing – original draft, C. S. – investigation, J. L. S. – investigation, E. M. L. - investigation, A. L. R. – investigation, L. H. D. – conceptualization, project administration, funding acquisition, writing – review and editing.

Conflicts of interest

There are no conflicts to declare.

Acknowledgements

We are grateful to the National Science Foundation (NSF, CHE 2102532 to LHD), to the National Institutes of Health (S10OD028585 for SCXR diffractometer), to the Boston University Undergraduate Research Opportunity Program (BU UROP to EML), and to Boston University Post-Doctoral Faculty Fellowship (BU Postdoctoral Faculty Fellowship to JLS) for their support of this work. We would also like to thank Dr Jeffrey Bacon and Dr William Tucker for helpful discussions.

Notes and references

1 H. Kuhn, S. Banthiya and K. van Leyen, *Biochim. Biophys. Acta*, 2015, **1851**, 308–330.
2 A. Wennman, A. Magnuson, M. Hamberg and E. H. Oliw, *J. Lipid Res.*, 2015, **56**, 1606–1615.
3 E. H. Oliw, *Prostaglandins Other Lipid Mediators*, 2002, **68–69**, 313–323.
4 Y. Umena, K. Kawakami, J.-R. Shen and N. Kamiya, *Nature*, 2011, **473**, 55–60.
5 K. N. Ferreira, T. M. Iverson, K. Maghlaoui, J. Barber and S. Iwata, *Science*, 2004, **303**, 1831.
6 J. Azadmanesh and G. E. O. Borgstahl, *Antioxidants*, 2018, **7**(2), 25–41.
7 H. Isobe, M. Shoji, T. Suzuki, J.-R. Shen and K. Yamaguchi, *J. Photochem. Photobiol., A*, 2021, **405**, 112905.
8 D. B. Rice, A. A. Massie and T. A. Jackson, *Acc. Chem. Res.*, 2017, **50**, 2706–2717.
9 A. S. Borovik, *Chem. Soc. Rev.*, 2011, **40**, 1870–1874.
10 Y.-R. Luo, *Handbook of Bond Dissociation Energies in Organic Compounds*, CRC Press LLC, 2002.
11 M.-H. Baik, M. Newcomb, R. A. Friesner and S. J. Lippard, *Chem. Rev.*, 2003, **103**, 2385–2420.
12 Z. Shirin, B. S. Hammes, V. G. Young and A. S. Borovik, *J. Am. Chem. Soc.*, 2000, **122**, 1836–1837.
13 Z. Shirin, B. S. Hammes, V. G. Young and A. S. Borovik, *J. Am. Chem. Soc.*, 2000, **122**(8), 1836–1837.
14 D. C. Cummins, J. G. Alvarado, J. P. T. Zaragoza, M. Q. Effendy Mubarak, Y.-T. Lin, S. P. de Visser and D. P. Goldberg, *Inorg. Chem.*, 2020, **59**, 16053–16064.
15 G. B. Wijeratne, B. Corzine, V. W. Day and T. A. Jackson, *Inorg. Chem.*, 2014, **53**, 7622–7634.
16 M. K. Coggins, L. M. Brines and J. A. Kovacs, *Inorg. Chem.*, 2013, **52**, 12383–12393.
17 X. Wu, M. S. Seo, K. M. Davis, Y.-M. Lee, J. Chen, K.-B. Cho, Y. N. Pushkar and W. Nam, *J. Am. Chem. Soc.*, 2011, **133**, 20088–20091.
18 C. R. Goldsmith, A. P. Cole and T. D. P. Stack, *J. Am. Chem. Soc.*, 2005, **127**, 9904–9912.
19 R. L. Halbach, D. Gygi, E. D. Bloch, B. L. Anderson and D. G. Nocera, *Chem. Sci.*, 2018, **9**, 4524–4528.
20 K.-B. Cho, S. Shaik and W. Nam, *J. Phys. Chem. Lett.*, 2012, **3**, 2851–2856.
21 A. Grass, D. Wannipurage, R. L. Lord and S. Groysman, *Coord. Chem. Rev.*, 2019, **400**, 213044.
22 A. Nandy and H. J. Kulik, *ACS Catal.*, 2020, **10**, 15033–15047.
23 J. K. Elinburg and L. H. Doerrer, *Polyhedron*, 2020, **190**, 114765.
24 J. L. Steele, L. Tahsini, C. Sun, J. K. Elinburg, C. M. Kotyk, J. McNeely, S. A. Stoian, A. Dragulescu-Andrasi, A. Ozarowski, M. Ozerov, J. Krzystek, J. Telser, J. W. Bacon, J. A. Golen, A. L. Rheingold and L. H. Doerrer, *Chem. Commun.*, 2018, **54**, 12045–12048.
25 L. Tahsini, S. E. Specht, J. S. Lum, J. J. M. Nelson, A. F. Long, J. A. Golen, A. L. Rheingold and L. H. Doerrer, *Inorg. Chem.*, 2013, **52**, 14050–14063.
26 J. S. Lum, L. Tahsini, J. A. Golen, C. Moore, A. L. Rheingold and L. H. Doerrer, *Chem.–Eur. J.*, 2013, **19**, 6374–6384.
27 S. A. Cantalupo, S. R. Fiedler, M. P. Shores, A. L. Rheingold and L. H. Doerrer, *Angew. Chem., Int. Ed.*, 2012, **51**, 1000–1005.
28 S. A. Cantalupo, H. E. Ferreira, E. Bataineh, A. J. King, M. V. Petersen, T. Wojtasiewicz, A. G. DiPasquale, A. L. Rheingold and L. H. Doerrer, *Inorg. Chem.*, 2011, **50**, 6584–6596.
29 S. A. Cantalupo, J. S. Lum, M. C. Buzzeo, C. Moore, A. G. Di Pasquale, A. L. Rheingold and L. H. Doerrer, *Dalton Trans.*, 2010, **39**, 374–383.
30 H. Hirao, L. Que Jr., W. Nam and S. Shaik, *Chem.–Eur. J.*, 2008, **14**, 1740–1756.
31 J. K. Elinburg, S. L. Carter, J. J. M. Nelson, D. G. Fraser, M. P. Crockett, A. B. Beeler, E. Nordlander, A. L. Rheingold and L. H. Doerrer, *Inorg. Chem.*, 2020, **59**, 16500–16513.
32 C. J. Willis, *Coord. Chem. Rev.*, 1988, **88**, 133–202.
33 S. E. N. Brazeau and L. H. Doerrer, *Dalton Trans.*, 2019, **48**, 4759–4768.

34 S. Hong, Y.-M. Lee, M. Sankaralingam, A. K. Vardhaman, Y. J. Park, K.-B. Cho, T. Ogura, R. Sarangi, S. Fukuzumi and W. Nam, *J. Am. Chem. Soc.*, 2016, **138**, 8523–8532.
35 H. M. Neu, R. A. Baglia and D. P. Goldberg, *Acc. Chem. Res.*, 2015, **48**, 2754–2764.
36 M. Mondal and U. Bora, *RSC Adv.*, 2013, **3**, 18716–18754.
37 T. J. Hubin, J. M. McCormick, N. W. Alcock and D. H. Busch, *Inorg. Chem.*, 2001, **40**, 435–444.
38 J. P. T. Zaragoza, M. A. Siegler and D. P. Goldberg, *J. Am. Chem. Soc.*, 2018, **140**, 4380–4390.
39 M. Sankaralingham, Y-M. Lee, D. G. Karmalkar, W. Nam and S. Fukuzumi, *J. Am. Chem. Soc.*, 2018, **140**(40), 12695–12699.
40 W. H. Harman and C. J. Chang, *J. Am. Chem. Soc.*, 2007, **129**, 15128–15129.
41 T. H. Parsell, M.-Y. Yang and A. S. Borovik, *J. Am. Chem. Soc.*, 2009, **131**, 2762–2763.
42 S. K. Barman, J. R. Jones, C. Sun, E. A. Hill, J. W. Ziller and A. S. Borovik, *J. Am. Chem. Soc.*, 2019, **141**, 11142–11150.
43 R. G. Agarwal, S. C. Coste, B. D. Groff, A. M. Heuer, H. Noh, G. A. Parada, C. F. Wise, E. M. Nichols, J. J. Warren and J. M. Mayer, *Chem. Rev.*, 2022, **122**, 1–49.
44 F. G. Bordwell, J. P. Cheng and J. A. Harrelson, *J. Am. Chem. Soc.*, 1988, **110**, 1229–1231.
45 D. B. Rice, G. B. Wijeratne, A. D. Burr, J. D. Parham, V. W. Day and T. A. Jackson, *Inorg. Chem.*, 2016, **55**, 8110–8120.